

SPICA Force Field for Lipid Membranes: Domain Formation Induced by Cholesterol

Sangjae Seo¹ and Wataru Shinoda^{1}*

¹ Department of Materials Chemistry, Nagoya University, Furo-cho, Chikusa-ku, Nagoya,
464-8603, Japan

*Email: w.shinoda@chembio.nagoya-u.ac.jp

ABSTRACT

Heterogeneity is essential for multicomponent lipid membranes. Especially, sterol-induced domain formation in membranes has recently attracted attention because of its biological importance. To investigate such membrane domains at molecular level, coarse-grained molecular dynamics (CG-MD) simulations are a promising approach since they allow to consider the temporal and spatial scales involved in domain formation. In this paper, we present a new CG force field, named SPICA, which can accurately predict domain formation within various lipids in membranes. The SPICA force field was developed as an extension of a previous CG model, known as SDK (Shinoda-DeVane-Klein), in which membrane properties such as tension, elasticity, and structure are well reproduced. By examining domain formation in a series of ternary lipid bilayers, we observed a separation into liquid-ordered and liquid-disordered phases fully consistent with experimental observations. Importantly, it is shown that the SPICA force field can detect the different phase behavior that results from subtle differences in the lipid composition of the bilayer.

INTRODUCTION

Cellular membranes are composed of various lipids and proteins. Accumulated evidences suggest that membrane constituents are not randomly mixed, but heterogeneously distributed¹⁻². Especially, the high affinity of cholesterol (CHOL) for saturated lipids induces phase separation, into liquid-ordered (Lo) and liquid-disordered (Ld) phases³⁻⁴, in membranes. Since the coexistence of Lo and Ld phases plays an important role in biological processes, such as cell signaling, sorting, and membrane fusion⁵⁻⁸, the formation of membrane domains driven by CHOL is a process of great interest. Several researchers have experimentally detected domain formation in model vesicles. Macroscopic phase separation has been directly observed using fluorescence microscopy⁹⁻¹⁰, and other spectroscopic techniques could also detect the existence of domains¹¹⁻¹⁴. In addition, the presence of domains enriched in CHOL and sphingolipids, known as lipid rafts, has been postulated¹⁵. However, since lipid rafts are dynamic domains and assumed to have submicron scales, the presence of lipid rafts *in vivo* is still unclear¹⁶⁻¹⁷.

To complement experiments, lipid membranes were also investigated by means of molecular dynamics (MD) simulations. Atomistic simulations were employed to characterize the physical and structural properties of lipids in atomic detail. In addition, the development of accurate all-atom (AA) force fields enabled us to address various membrane problems. For example, the propensity of hydrogen bond formation between sphingomyelin (SM) and CHOL was studied using the CHARMM¹⁸⁻¹⁹ and Slipid²⁰ force fields. In addition, AA-MD simulations probed features of lipid rafts, such as condensed packing and increased rigidity²¹⁻²². However, because of the computational cost of these simulations, the accessible simulation time using AA force fields was limited to the early stage of phase separation, and it was difficult to observe the fully separated state. Coarse-grained (CG) models readily extended the simulation time by reducing the degrees of freedom of the system and allowing a larger integration time step. The MARTINI force field is one of the most widely used CG force fields in membrane studies²³⁻²⁴. It was firstly employed to conduct the phase separation of a 1,2-dipalmitoyl-sn-glycero-3-phosphocholine (DPPC)/1,2-dilinoleoyl-sn-glycero-3-phosphocholine (DLiPC)/CHOL ternary bilayer²⁵. Subsequent CG simulations using the MARTINI force field investigated the characteristics of lipid domains²⁶⁻²⁸. Shinoda *et al.* proposed a different CG force field, which was designed to reproduce thermodynamic properties such as surface/interfacial tension and density²⁹⁻³⁰. A recent extension of this force

field included CHOL for phase separation studies³¹. Although these CG force fields successfully simulated domain formation in membranes, further optimization and development is still required to improve their accuracy. For example, MARTINI could not reproduce the phase separation experimentally detected in a DPPC/1,2-dioleoyl-sn-glycero-3-phosphocholine (DOPC)/CHOL bilayer³². Besides, despite the importance of SM in domain formation, to our knowledge, there is not an accurate CG SM model.

In this paper, we present an optimized CG lipid force field coined SPICA (Surface Property fitting Coarse grAining). The SPICA force field is developed based on the previous CG model by Shinoda *et al.*^{29-31,33-36}, which is often called SDK (Shinoda-DeVane-Klein). Most of the lipid parameters were adopted from the conventional SDK force field and the parameters of new CG beads were determined by the same strategy of SDK model. In addition, CHOL parameters were further optimized to accurately predict the experimentally known phase behavior of lipid mixtures. Although the previous SDK CHOL model³¹ succeeded in showing membrane domain formation in a ternary mixture, the miscibility temperature was underestimated and the partitioning of CHOL into different domains was poorly described. To solve these issues, we considered distribution functions on top of thermodynamic quantities in the optimization process. In addition, we have increased the number of lipids in the available library within the SPICA force field. Since many experimental studies of lipid domain formation have been performed on lipid mixtures containing SM, we have developed a SM model, which should be useful to address questions related to the lipid raft hypothesis. Features of SM membranes, such as hydrogen bonding and dense packing, were considered. Polyunsaturated lipids were also added to the SPICA lipid library for a variety of applications. We have conducted AA-MD simulations, extensively validated by their comparison with experimental results, to yield the reference data for CG modeling. To test this new CG lipid force field, we simulated several ternary bilayers: DPPC/DOPC/CHOL, DPPC/DLiPC/CHOL, N-stearoyl-D-erythro-sphingosylphosphorylcholine (SSM)/DOPC/CHOL, and SSM/POPC/CHOL. The phase behaviors of these ternary bilayers were examined and validated by comparing with experimental results.

METHODS

All-atom molecular dynamics

We performed AA-MD simulations to produce reference data for CG modeling. AA-MD simulations were conducted using NAMD³⁷ with the latest version of the CHARMM 36 (C36) force field^{18,38-40}. All simulations were carried out in the NPT ensemble. Langevin dynamics with a 5 ps^{-1} damping coefficient was used to maintain a constant temperature for each system at 323 K. A Nosé-Hoover Langevin piston⁴¹ was used to maintain the pressure at 1 atm. The Langevin piston period and decay were set to 200 and 100 fs, respectively. For bilayer simulations, semi-isotropic coupling was used to control the cell fluctuations. The temperature was set above the main transition temperature of a pure lipid bilayer. The time step size for the integration of the equations of motion was 2 fs, and we performed at least 1 μs of MD simulation for each system to evaluate the equilibrated membrane properties. The first 50 ns of every trajectory were discarded as equilibration, and the last 950 ns were used for the analyses. For the SM membrane, the equilibration of the AA systems in the presence of CHOL required ca. 500 ns. Therefore, in these cases, only the last 500 ns were considered as production and used for the analyses. Long-range electrostatic interactions were taken into account by the particle mesh Ewald method⁴²⁻⁴³. Lennard-Jones interactions were smoothly truncated at a cutoff distance of 12 Å by applying a force-switching scheme in the range of 10 to 12 Å. We carried out a series of AA-MD simulations of lipid membranes containing CHOL at different CHOL/lipid molecular ratios (1:9, 2:8, 3:7, and 4:6) to evaluate the effect of CHOL on the membrane properties. We also conducted MD simulations of mixed lipid membranes without CHOL. Details of each system are given in Table S1. The initial configurations for the simulations were built with CHARMM-GUI⁴⁴.

Coarse-grained molecular dynamics

We have carried out all CG-MD using the LAMMPS software⁴⁵. Temperature (323 K, unless otherwise described) and pressure (1 atm) were controlled using a Nosé-Hoover thermostat⁴⁶⁻⁴⁷ and a Parrinello-Rahman barostat⁴⁸⁻⁴⁹, respectively. A semi-isotropic coupling scheme, where the pressures normal and lateral to the membrane are controlled separately, with a response time of 5 ps was employed. The long-range electrostatic interactions were calculated using the particle-particle particle-mesh (P3M) method⁵⁰. The simulation time step was set to 10 fs. In order to optimize the parameters for CHOL, we repeatedly performed 30 ns MD

simulations of a DOPC membrane containing 30% of CHOL. The membrane properties of the CG systems were calculated from the 500 ns simulation trajectories. In the CG-MD simulations for testing the domain formation in ternary lipid mixtures, 4 μ s-long MD simulations were conducted. In a series of MD simulations for optimizing the CG interaction parameters, fully hydrated lipid membrane systems containing 128 lipids were used. The initial configurations of the CG systems were prepared by mapping equilibrated AA snapshots into CG beads using the CG-it tool²⁴. To build the ternary mixtures, we constructed systems with unit cells having 300 lipids for each composition (Table S1) using CHARMM-GUI. Then, the initial configuration of every ternary mixture was prepared by replicating (3 \times 3) each of these unit cells in the directions lateral to the bilayer. For ternary mixtures, temperature was set to 298 K, which is below miscibility transition temperature⁹.

The coarse-grained model

The SPICA force field basically maps 3-4 heavy atoms into one CG bead. For example, three water molecules are represented by one CG water bead. The SPICA force field exploits the same functional form as the SDK model. The bonded interactions are described by conventional harmonic functions

$$\begin{aligned} U_{1-2} &= \sum_{\text{bond}} k_b (r_{ij} - r_0)^2 \\ U_{1-2-3} &= \sum_{\text{angle}} k_\theta (\theta_{ijk} - \theta_0)^2 \end{aligned} \quad (1)$$

where k_b and k_θ are the force constants and r_0 and θ_0 are the distance and angle at the energy minimum. Since these simple harmonic functions can only represent unimodal distributions, if the distribution obtained from the AA-MD simulation is bimodal, its average and dispersion values are targeted. A 1-3 correction term

$$U_{1-3}^{\text{correct}} = \sum_{1-3} [U_{nb}(r_{ij}) - U_{nb}(r_{\min})] \quad \text{for } r_{ij} < r_{\min} \quad (2)$$

is often required to avoid an angle collapse. The dihedral term has a form analogous to that found in the CHARMM force field,

$$U_{1-2-3-4} = \sum_{\text{dihed}} k_\phi [1 + \cos(n\phi_{ijkl} - d)] \quad (3)$$

The dihedral term is only used to better describe the conformational states of the CHOL tail. The nonbonded interactions are described by the familiar LJ and Coulomb potentials. The LJ potential has two different forms; the interactions involving water are modeled with the LJ12-4 function, while those involving any other pairs are described using the LJ9-6 function

$$U_{nb}(r_{ij}) = \begin{cases} \frac{3\sqrt{3}}{2} \varepsilon_{ij} \left[\left(\frac{\sigma_{ij}}{r_{ij}} \right)^{12} - \left(\frac{\sigma_{ij}}{r_{ij}} \right)^4 \right] & \text{for the pairs involving water} \\ \frac{27}{4} \varepsilon_{ij} \left[\left(\frac{\sigma_{ij}}{r_{ij}} \right)^9 - \left(\frac{\sigma_{ij}}{r_{ij}} \right)^6 \right] & \text{for any other pairs} \end{cases} \quad (4)$$

where σ_{ij} is the distance where the energy equals to zero, and ε_{ij} is the minimum energy. This separation is required to avoid freezing water and accurately reproduce the thermodynamic properties of the liquid state.^{29,30,34} The LJ interaction is simply truncated at 15 Å. The electrostatic interactions are described by typical Coulomb potentials

$$U_{elec}(r_{ij}) = \frac{1}{4\pi\varepsilon_0\varepsilon_r} \frac{q_i q_j}{r_{ij}} \quad (5)$$

For better accuracy, the SPICA force field does not truncate the electrostatic interactions at a given cut-off distance; the long-range electrostatic forces are instead calculated using a non-cutoff scheme like the P3M method⁵⁰. A relative dielectric constant value of $\varepsilon_r = 80$ is used to take into account the screening effect of water.

Phospholipid modeling

To extend the lipid library, we introduced new CG beads for SM and polyunsaturated lipids. Table 1 lists the CG beads newly developed in this work, and the CG mapping of each lipid is shown in Fig. 1.

Table 1. CG segment name and the corresponding all-atomic functional group

CG segment	all-atom
PEP	-CO-NH-
OAD	-CH-OH-

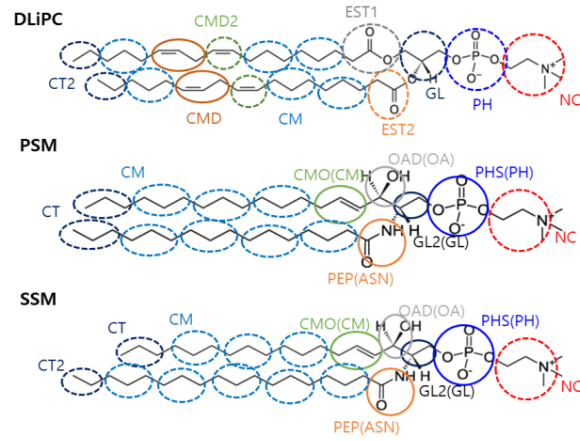


Figure 1. CG mapping of SSM, PSM, and DLiPC. Dashed line circles are bead types from the standard SDK force field, and solid line circles are newly introduced bead types. The names within parentheses indicate the bead types that, by analogy, we took from the previous force field^{30-31, 34-35}.

The bond stretching and angle bending parameters were fitted to reproduce the distribution functions obtained from AA simulations. For nonbonded interactions, we mostly adopted the parameters of similar, already existing, bead types^{29-31, 34-35}. For example, the parameters of the PEP and OAD beads were taken from the ASN³⁵ and OA²⁹ beads, respectively. The parameters were further tuned to precisely reproduce the correct membrane properties. It is worth noting that the phosphate group of SM is replaced by a new bead type PHS (-PO₄-(-1)). Although the chemical structure of the phosphate group is the same in SM and glycerolipids, the phosphate interaction of SM is somewhat different because the phosphate group in SM forms hydrogen bonds with the amide and hydroxyl groups. Thus, we renamed the phosphate bead (PH) to PHS, and slightly modified the phosphate interaction parameters of SM to satisfy electron density profile, and RDFs. For polyunsaturated lipids, we added a new bead type, CMD. Analogously to the other beads, the intramolecular parameters were determined using AA-MD results as reference. The nonbonded parameters were basically taken from the CMD2 bead (-HC=CH-), though the parameters were scaled to adjust the thermodynamic and structural properties of the membrane.

Cholesterol modeling

The definition of the CG segments and the topology of CHOL are the same as in the previous model³¹, in which the bond interaction parameters were fit to reproduce the distributions obtained from AA-MD simulations, and the LJ potentials were determined by targeting thermodynamic properties of small-molecule analogues. However, the cross interactions involving CHOL beads were fitted by comparison with those of particles chemically similar and already present in the previous CG parameter library. In this way, the structural properties of CHOL were treated with a lower priority; this resulted in a poor prediction of the CHOL partitioning in lipid mixtures. To optimize the cross interactions, we used the conventional combination rule and multiplied ε_{ij} by a scaling value. We repeatedly run 30 ns MD simulations of the DOPC/CHOL (30%) system using various scaling values and chose the set that better satisfied both the membrane properties and radial distributions obtained from an AA-MD simulation on the same system. This system was chosen to optimize the interactions of CHOL-CHOL and CHOL-phospholipid because the system could be quickly equilibrated, and DOPC contains both CM (-CH₂CH₂CH₂-) and CMD2 (-HC=CH-) beads for the lipid tail. Also sufficient CHOL molecules were needed to efficiently sample all relevant conformations in the short simulation time. The interaction between the CMD bead (-HC=CHCH₂-) for polyunsaturated lipid and CHOL was scaled from the CMD2 bead. The interactions between SM and CHOL were optimized by the same strategy in the system of SSM/CHOL (30%), but only the interactions between CHOL and new beads, such as GL2, PEP, and OAD, were tuned to satisfy the membrane properties.

Analyses

Analyses were performed with VMD⁵¹ and python codes written with SciPy, NumPy⁵², and MDAnalysis⁵³. To assess the CG parameters, we calculated the surface area per lipid (SA/lipid), membrane thickness, area compressibility modulus (K_A), and 2-dimensional radial distribution function (2D RDF). The SA/lipid was calculated by dividing the area of the membrane by the number of lipids in one leaflet. The membrane thickness was defined as the average distance (d_{P-P}) between the phosphate beads of the upper and lower lipid leaflets along the direction normal to the bilayer (z-axis). The area compressibility modulus was

calculated by

$$K_A = \frac{k_B T \langle A \rangle}{N \sigma_{\langle A \rangle}^2} \quad (6)$$

where k_B is the Boltzmann constant, and T is the temperature. $\langle A \rangle$ and $\sigma_{\langle A \rangle}^2$ indicate the average surface area and the dispersion, respectively. The segmental order parameter in the lipid tail was computed by

$$S_{ZZ} = \frac{\langle 3 \cos^2 \theta - 1 \rangle}{2} \quad (7)$$

where θ is the angle between the bond vectors in the hydrophobic lipid tails and the bilayer normal.

We calculated the flip-flop rate of CHOL according to the procedure in Ref. 54. The rate of flip-flop is determined by

$$k_{\text{flip}} = \frac{1}{k_f^{-1} + k_d^{-1}} \times \frac{1}{2} \quad (8)$$

where k_d is the rate CHOL moves from the bilayer center to the equilibrium position, and k_f is the rate CHOL moves from the equilibrium position to the membrane center. k_f can be calculated by

$$k_f = k_d \times \exp(-\Delta G_{\text{center}} / RT) \quad (9)$$

where ΔG_{center} is the free energy required to move CHOL from its equilibrium position in the bilayer to the bilayer center. To estimate k_d , we measured the time elapsed before CHOL recovers its equilibrium position from the bilayer center. We run MD simulations for 2 μs to obtain enough sampling of the events. We estimated ΔG_{center} from the probability density of the hydroxyl group of CHOL (OAB bead) along the z -axis as follows:

$$\Delta G_{\text{center}} = -RT \ln \frac{\rho_{\text{OAB}}(z_{\text{center}})}{\rho_{\text{OAB}}(z_{\text{eq}})} \quad (10)$$

For the phase separation simulations, we quantified the enrichment of CHOLs in the saturated

lipid regions. In order to identify its neighboring lipid within the lipid leaflet, we used a 2-dimensional Voronoi tessellation by selecting PH (phosphate) and OAB (hydroxyl) beads as references for lipids and CHOL positions, respectively.⁵⁵ Based on this tessellation, we counted the number of CHOL-saturated lipid ($N_{chol-sat}$) and CHOL-unsaturated lipid ($N_{chol-unsat}$) contacts. The fraction of CHOL-saturated lipid contacts was measured as follows:

$$\Phi_C = \frac{N_{chol-sat}}{N_{chol-sat} + N_{chol-unsat}} \quad (11)$$

RESULTS and DISCUSSION

Sphingomyelin and polyunsaturated lipid modeling

We newly modeled SM and DLiPC lipids to address various phase separation problems. The bonded parameters were tuned to reproduce the bond and angle distributions obtained from AA-MD simulations (Figs. S1 and S2). Table 2 summarizes the calculated membrane properties. For the parameterization, we chose SSM because it contains all the bead types of lipid tail required to easily extend the acyl chain of SM. Indeed, the membrane properties of both SSM and N-palmitoyl-D-erythro-sphingosylphosphorylcholine (PSM) evaluated from simulations performed using the present CG model are in good agreement with those obtained from AA-MD simulations. The area compressibility modulus computed using the present CG model deviates from that calculated using the atomistic force field. However, considering the large statistical error of the AA-MD simulations, the discrepancy between AA- and CG-MD simulation results is not excessively significant. Moreover, the area compressibility modulus of SSM calculated in previous studies¹⁸ shows a value similar to that obtained with our CG model. Thus, we consider that the area compressibility modulus is within a reasonable range. The CG segmental order parameter (Fig. S3) and electron density profiles (Fig. S4) were calculated and show good agreement with the corresponding AA simulation results.

Table 2. Calculated membrane properties.

Lipid	SA/lipid [\AA^2]		Thickness, d_{p-p} [\AA]		K_A [mN/m]	
	AA	CG	AA	CG	AA	CG
SSM	54.4	57.2	43.1	41.4	266 (50), 440 (60) ^a	460 (15)
PSM ^b	55.4	56.8	40.7	39.6	350 (50)	460 (15)
DLiPC	70.2	71.3	36.9	36.9	263 (10)	357 (5)

* Numbers within parentheses indicate standard errors.

^a The PSM data (produced at 48 °C) and K_A value for SSM are taken from Ref. 18.

Cholesterol model optimization

Crystal structure

The lattice cells parameters of CHOL crystal structure were estimated from simulations performed in an anhydrous environment to assess the structural properties of the CHOL model. The anhydrous CHOL model was prepared based on the experimental crystallographic data (Fig. S5). Both CG- and AA-MD simulations were conducted on a triclinic cell at 310 K. Table 3 compares the experimental crystallographic data of CHOL with those obtained from the MD simulations. The lattice vectors calculated from the MD simulation show an overall good agreement with the experimental crystallographic data, except for the SDK CHOL model. The values calculated using the SDK CHOL model show a large deviation from the experiment. This deviation is significantly reduced throughout the optimization process. The relative errors between the experimental values and those obtained from the CG-MD simulation using SPICA force field are within 5% with the exception of the γ value. The small error was inevitable because we optimized the CHOL parameters against membrane properties, not to reproduce individual RDFs; furthermore, the parameterization was performed in a DOPC membrane, not in an anhydrous environment. Nevertheless, our CG model reproduces well the lattice cell parameters found in the experimental crystal structure.

Table 3. Lattice cell parameters for cholesterol crystal structure.

	Experiment ^a	AA ^b	CG ^b	
			SDK CHOL model ³¹	Current work
a (Å)	27.565	27.898 ± 0.009	32.311 ± 0.135	26.817 ± 0.024
b (Å)	38.624	35.904 ± 0.007	30.722 ± 0.118	36.783 ± 0.013
c (Å)	10.758	10.731 ± 0.003	10.534 ± 0.009	10.723 ± 0.008
α (°)	93.49	93.513 ± 0.008	89.848 ± 0.025	92.815 ± 0.055
β (°)	90.90	90.882 ± 0.004	90.151 ± 0.017	93.940 ± 0.056
γ (°)	117.15	119.662 ± 0.009	143.208 ± 0.210	108.380 ± 0.042

^a Data taken from Ref. 56.

^b MD simulation data were calculated from a 50-ns trajectory.

Membrane properties

Physical and structural properties of lipid membranes containing different amounts of CHOL were evaluated to assess the quality of the optimized CHOL CG model. The membrane properties were evaluated using 1 μ s AA- and CG-MD simulations. We confirmed the equilibration of the systems by the convergence of the membrane area. Fig. S6 shows the time evolution of the membrane area along the MD simulations. For both AA- and CG-MD simulations, the surface areas were well converged within the simulation time. The last 500 ns of the trajectories were used for the analyses.

Figure 2 displays fundamental properties of DPPC, DOPC, and SSM membranes (membrane area, thickness, and area compressibility modulus) as a function of CHOL concentration. The membrane properties calculated from the CG-MD simulations show an overall good agreement with those obtained from the AA-MD simulations, though slight deviations can be observed. It is well known that lipid tails are tightly packed in the presence of CHOL because of the rigid steroid ring structure. To identify the lipid packing status, we calculated the SA/lipid. The SA values estimated from CG-MD nicely follow the trend of the AA simulation results. As CHOL content increases, the SA/lipid decreases. This clearly indicates that the hydrophobic chains of the membrane lipids are tightly packed in the presence of CHOLs. A slightly smaller membrane thickness was calculated from the CG-MD simulations in

comparison with that obtained from the AA-MD trajectories, though the increase in the thickness with the CHOL content is well captured by the CG-MD. An additional feature of CHOL is that it increases the rigidity of the membrane. The calculated area compressibility moduli also show good agreement with those obtained from the AA-MD simulations. Especially, the significant increase in the rigidity of the membrane at high CHOL concentration was well reproduced by the present CG model.

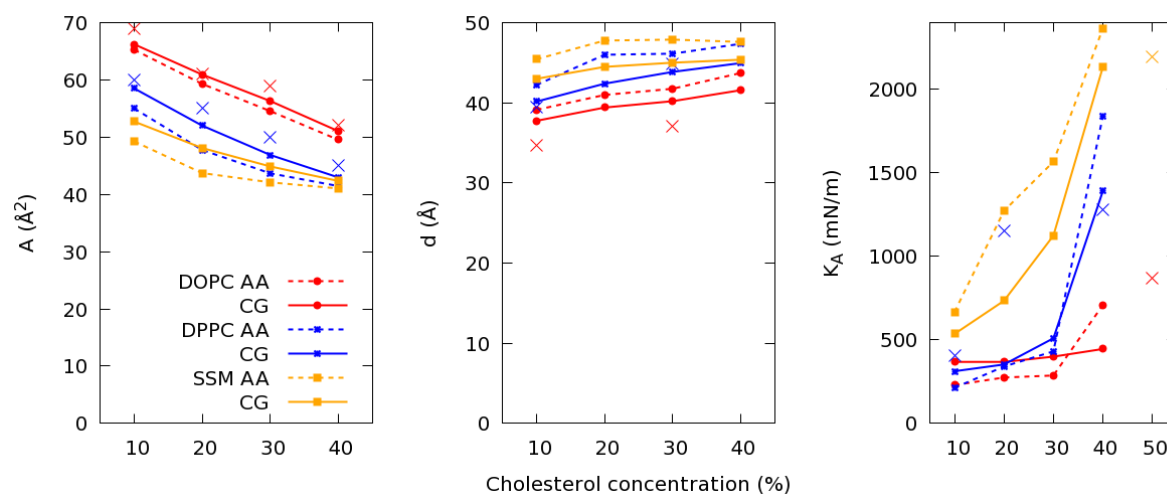


Figure 2. Membrane area (A), thickness (d), and area compressibility modulus (K_A) as a function of cholesterol content. The standard errors of SA/lipid and membrane thickness are smaller than the symbols. The corresponding experimental values, if available, are plotted as cross symbols⁵⁷⁻⁶¹.

Radial distribution function

The CHOL model was optimized to provide a reasonable structure and distribution of CHOL in multicomponent lipid membranes. We evaluated 2D RDFs between the center of masses of the lipids in the membranes rather than conventional RDF between beads.

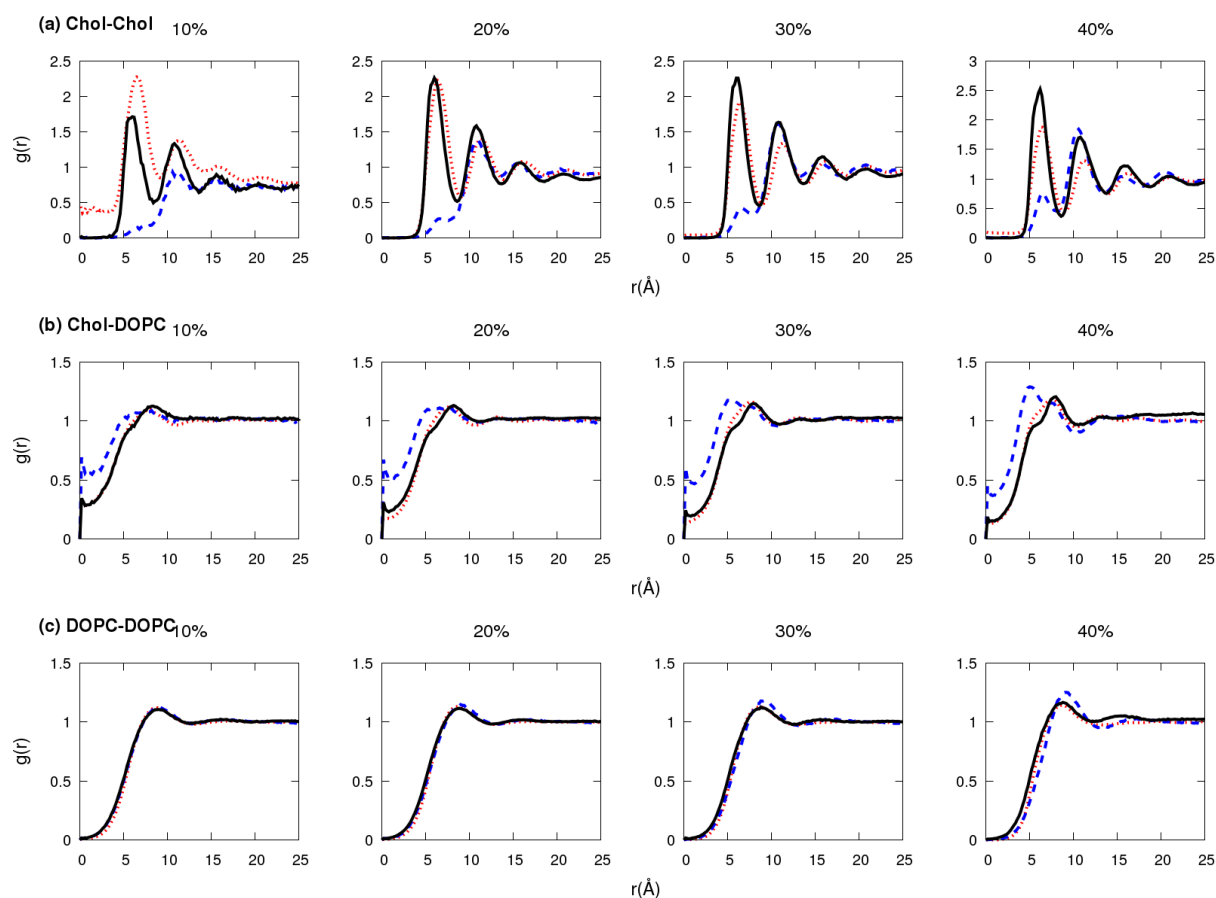


Figure 3. Two-dimensional radial distribution functions of DOPC/CHOL membranes with different CHOL content. The red dotted and blue dashed lines are the 2D RDF calculated from the AA-MD simulation and using the previous version of the CG force field, respectively. The black solid line is the result with the present CG model. (a) CHOL-CHOL, (b) CHOL-DOPC, and (c) DOPC-DOPC RDFs.

Figure 3 shows the 2D RDFs between the center of masses of the lipids in DOPC/CHOL membranes at different CHOL concentrations. 2D RDF plots for DPPC/CHOL and SSM/CHOL are given in the SI (Figs. S7 and S8). The 2D RDFs obtained with the previous CHOL CG model significantly deviate from those obtained using the atomistic force field. In particular, the first peak of the CHOL-CHOL RDF, found near 6 Å, is largely underestimated when using the previous CG model for CHOL. Moreover, if CHOL concentration is 10%, this first peak is hardly found. Moreover, the shape of the CHOL-DOPC RDF, obtained when the previous version of the CG force field is employed, is inconsistent with the AA-MD result. We suspected that the incorrect partitioning of CHOL in the ternary mixtures resulted from the poor description of the 2D RDFs. Thus, we paid attention to improve these 2D RDFs during the optimization process. As a consequence, the present CG model gives results that

are in good agreement with those obtained from AA-MD and reasonably predicts CHOL molecular partitioning. The overall shape and height of the peaks in the CHOL-CHOL RDF are well reproduced by the present CG model. This is more evident in the CHOL-DOPC 2D RDF. The distributions obtained by the present CG parameter set almost coincide with those calculated using AA-MD. The DOPC-DOPC RDF does not show significant changes as the CG parameters for the DOPC-DOPC interaction were not modified. In the case of DPPC/CHOL membranes, the overall agreement between the 2D RDFs computed using the present CG model and the atomistic force field is again very good. Only a minor difference can be observed in the CHOL-DPPC 2D RDF, in which the first and second peaks are slightly underestimated and overestimated, respectively (Fig. S7(a)). Similarly, the RDFs of the SSM/CHOL mixture obtained using the present CG model show a good agreement with those calculated from the AA-MD simulations. Although the second peak in the CHOL-SM RDF exhibits a slight deviation from that calculated using the atomistic force field, the overall shape and height of the peaks in the 2D RDFs are well reproduced by the present CG model.

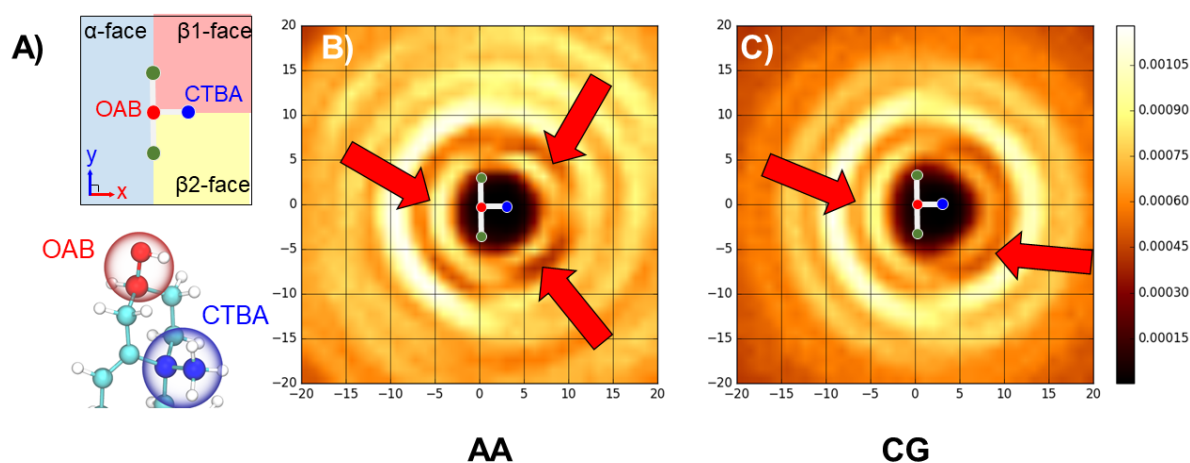


Figure 4. In-plane probability distribution of CHOLs. (a) Schematic description of the orientation. The vector connecting OAB (the bead including the hydroxyl group) and CTBA (the bead including the protruded methyl group) is aligned with the x-axis. The α -face is on the smooth flat surface of CHOL, and the β -face is on the same side as the out-of-plane methyl groups. (b, c) 2-dimensional probability distribution of center of mass of CHOL with respect to the reference orientation. (b) AA-MD simulation shows the three-fold symmetry axis indicated by the red arrows. (c) CG-MD simulation shows the two-fold symmetry.

In addition to the 2D RDFs, we also analyzed the in-plane probability distribution of CHOL to assess the orientational arrangement of CHOL in bilayer membranes. CHOL has an asymmetric structure characterized by a smooth α -face and a rough β -face. Martinez-Seara *et al.*⁶² showed that the spatial distribution of CHOL has a three-fold symmetry that results from CHOL structure. To verify our model, the two-dimensional distributions of the center of mass of CHOL molecules with respect to a reference orientation were calculated. In our calculation, the reference orientation was determined by centering the OAB bead at the origin and aligning the x-axis with the OAB-CTBA vector. For the consistency of the CG- and AA-MD simulation results, the AA trajectory was mapped to the CG representation, and the distribution was analyzed. Figure 4 displays the in-plane probability distribution of CHOL in a DPPC bilayer with 20% CHOL. The AA simulation result shows the trilobed coordination shells. The first shell locates at ~ 5 Å, and the highlights at the α -, $\beta 1$ -, and $\beta 2$ -faces demonstrate the three-fold symmetry of the CHOL distribution. Compared with the AA-MD simulation, our CG model reproduces fairly well the in-plane distribution. It shows the three distinctive coordination shells. As one can also see in the 2D RDF plots, the locations of the shells in the CG model almost coincide with those found when using the atomistic model. The peak at the α -face is well reproduced by the present CG CHOL model, but there is not a clear separation into $\beta 1$ -face and $\beta 2$ -face. Despite the two-fold symmetry at the first coordination shell, the overall distribution of CHOL is well described by the present CG model.

Order parameter

Deuterium order parameter has been widely used to evaluate the quality of trajectories generated from AA-MD simulations. The C36 force field has been extensively examined, and it has been proven to give a reasonable order parameter profile when compared to NMR results^{18, 39, 63}. Since the CG model cannot yield a deuterium order parameter directly comparable to the NMR results, we mapped the AA-MD trajectory to the corresponding CG sites and calculated the segmental order parameter for the hydrophobic tails using Eq. (7). Figure 5 displays the calculated order parameters for various lipids in mixtures with different CHOL content. The ordering effect of CHOL is reproduced by the present CG model as the order parameter increases with CHOL concentration. Although the values calculated with the present CHOL model are slightly lower than those obtained from the AA-MD trajectories, the

AA and CG order parameter profiles present an overall good agreement. Moreover, the higher acyl chain order of SM in comparison with glycerolipid is well reproduced by the present CG model.

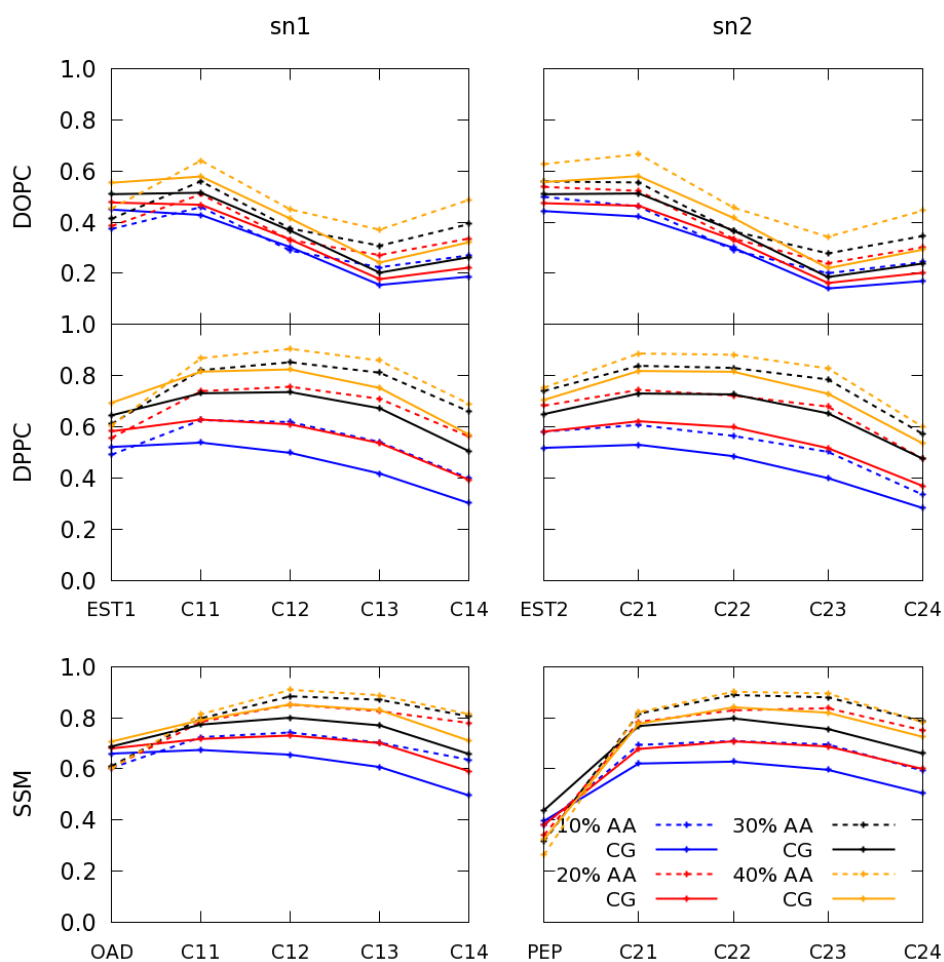


Figure 5. CG order parameters of various lipids in mixtures with different CHOL content. The dashed and solid lines indicate AA- and CG-MD results, respectively. The color code is presented in the SSM-sn2 plot.

Cholesterol flip-flop

One of the distinguishable features of CHOL is its higher flip-flop rate in comparison with that of phospholipids. Several experimental studies have measured the flip-flop rate of CHOL. Because of the limitations, such as time resolution, of these measurements, the reported flip-

flip rate shows a large uncertainty: the reported half-life times of CHOL are in the range of seconds⁶⁴⁻⁶⁵ to hours⁶⁶⁻⁶⁷. AA-MD simulations and theoretical studies were also undertaken to investigate the flip-flop pathway of CHOL, typically predicting a flip-flop rate higher than that experimentally reported⁶⁸⁻⁶⁹. A commonly observed trend is that, compared with phospholipids, CHOLs show rapid flip-flop motion. Here, we measured the flip-flop rate using the method employed in Ref. 44.

Table 4. Calculated flip-flop rates.

	k_d (s ⁻¹)	k_f (s ⁻¹)	Flip-flop rate (s ⁻¹)
DPPC+CHOL 20%	8.72×10^7 to 1.95×10^8	3.46×10^4 to 6.74×10^4	1.73×10^4 to 3.37×10^4
DPPC+CHOL 40%	7.91×10^6 to 1.78×10^8	7.31×10^2 to 1.48×10^3	3.65×10^2 to 7.43×10^2
DOPC+CHOL 20%	1.62×10^8 to 1.76×10^8	2.88×10^5 to 3.52×10^5	1.43×10^5 to 1.76×10^5
DOPC+CHOL 40%	1.19×10^6 to 2.09×10^8	3.63×10^4 to 5.84×10^4	1.81×10^4 to 2.92×10^4
SSM+CHOL 20%	7.99×10^6 to 4.35×10^7	1.28×10^3 to 2.61×10^3	6.41×10^2 to 1.30×10^3
SSM+CHOL 40%	NA	NA	NA

Table 4 lists the flip-flop rates of CHOL calculated from 2 μ s CG-MD simulations using the present CG parameter set. To achieve better statistics, we have run 10 independent MD simulations, started from different initial configurations, for each lipid mixture. The ranges in the table indicate the highest and lowest rates calculated from our simulations. The calculated rates are similar to the values obtained from atomistic MD using the GROMOS87 force field (*i.e.*, DPPC with 40% CHOL: 9.4 to 5.0×10^2 s⁻¹), while they are much lower, by one or two orders of magnitude, than those obtained using the MARTINI model (*i.e.*, DPPC with 40% CHOL: 7.2×10^3 to 2.5×10^4 s⁻¹). As the flip-flop rate rather sensitively varies depending on the experimental measurements and conditions, it is difficult to give a precise discussion on the accuracy. However, considering that the lower limit of the half-life time measured from experiments is <1 s, the flip-flop rate obtained by the present SPICA force field is within a reasonable range (*i.e.*, the estimated half-life time of DPPC with 40% CHOL is ~ 1 ms). Furthermore, the flip-flop rate tendency is consistent with that found in other studies⁷⁰⁻⁷¹ as the unsaturated lipids show the fastest flip-flop rate. Interestingly, although the structure of the lipid tails of SSM and DPPC is similar, SSM shows a lower flip-flop rate than DPPC. This reflects the strong affinity of CHOL for SM. The strong interaction between SSM and

CHOL due to hydrogen bonding may slow down the flip-flop motions. In the SSM membrane with 40% CHOL, we could not observe any flip-flop event during the 2 μs simulation.

Phase separation simulations

Although the previous CHOL model successfully induced phase separation in a ternary mixed membrane of 1,2-diarachidoyl-sn-glycero-3-phosphocholine (DAPC)/DOPC/CHOL, CHOL was found to be uniformly distributed over the membrane irrespective of the phase where it was located. Moreover, the miscibility transition temperature was significantly underestimated: the phase separation took place at a much lower temperature than in experiments. To fix these issues, we have optimized the interaction parameters to obtain a CHOL model with better structural properties and reasonable thermodynamic properties such as interfacial tension and density. We have tested the present SPICA force field by conducting phase separation simulations for various ternary mixtures.

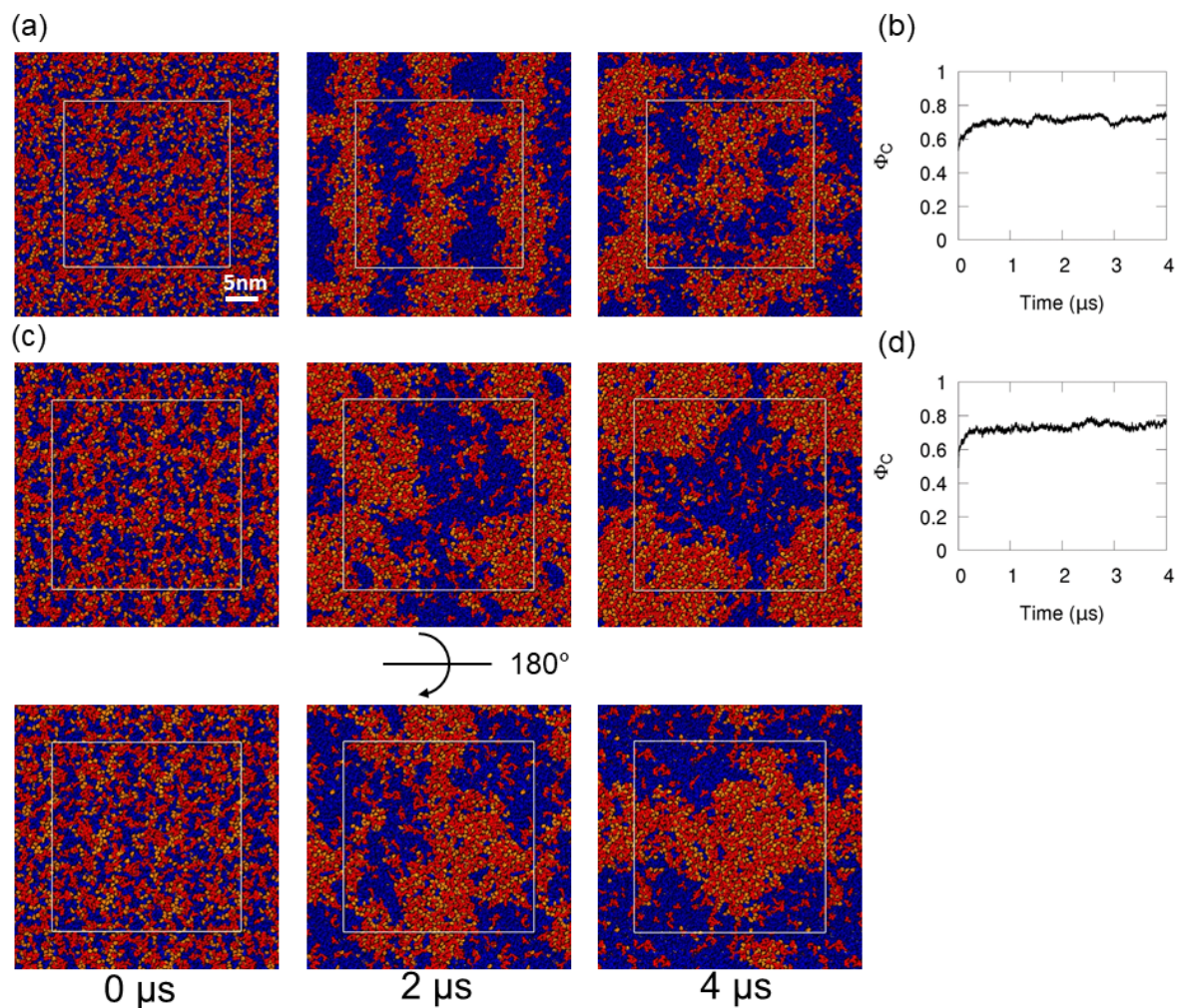


Figure 6. Phase separation simulation of DPPC/DOPC/CHOL (a and b) and DPPC/DLiPC/CHOL (c and d) mixtures. White boxes represent the periodically repeated simulation boxes. (a) Snapshots of the DPPC/DOPC/CHOL membrane at 0 μ s, 2 μ s, and 4 μ s. Color code is as follows: red, blue, and orange represent DPPC, DOPC, and CHOL, respectively. (c) Snapshots of the DPPC/DLiPC/CHOL membrane at 0 μ s, 2 μ s, and 4 μ s. The first and second rows show the upper and lower leaflets of the membrane, respectively. Color code is as follows: red, blue, and orange represent DPPC, DLiPC, and CHOL, respectively. (b and d) Calculated fraction of contacts between DPPC and CHOL.

First, we performed a 4 μ s simulation of DPPC:DOPC:CHOL in a 1:1:1 ratio. In phase separation experiments, this mixture has been widely used as a model vesicular system, showing macroscopic domain formation over the vesicle^{9,12}. However, CG simulations with the MARTINI force field failed to reproduce the phase separation shown by this mixture³². Figure 6(a) illustrates the development of domain formation in the mixed membrane in the course of the CG-MD with the present CG model. As time elapses, the initially mixed membrane is separated into Lo and Ld phases; the Lo region is enriched in CHOLs and DPPC, while the Ld region is dominated by DOPC. After 2 μ s, domain formation was quite evident. Unlike what happened with the previous CHOL model³¹, the preferred partitioning of CHOLs into the Lo region is clearly observed when using the present CG model. To quantify the preference of CHOL for the DPPC region, we calculated the fraction of CHOL-DPPC contacts. As Fig. 6(b) shows, the value of this fraction started at around 0.5, indicating fully mixed state at the beginning, and later increased and saturated at around 0.72, which indicates the enrichment of CHOL in the DPPC dominated domain.

Previous studies demonstrated that polyunsaturated lipids promote the lateral segregation into Lo and Ld domains^{28, 72}. A ternary mixture of DPPC:DLiPC:CHOL in a 1:1:1 ratio was prepared and simulated for 4 μ s. Fig. 6(c)-(d) demonstrate the phase separation of this mixture. Intriguingly, it shows antiregistered domain formation, in which the opposing leaflets are in different phases. When the thicknesses of the Lo and Ld domains are largely different, the domains are antiregistered to prevent the energy penalty due to a significant hydrophobic mismatch energy²⁷. In the absence of CHOL, the membrane thickness of DLiPC is about 37 Å, whereas the membrane thickness of DPPC increases over 44 Å in the presence of CHOL. Thus, we surmise that the hydrophobic mismatch between Lo and Ld domains

induced the antiregistered domain formation observed in our simulation.

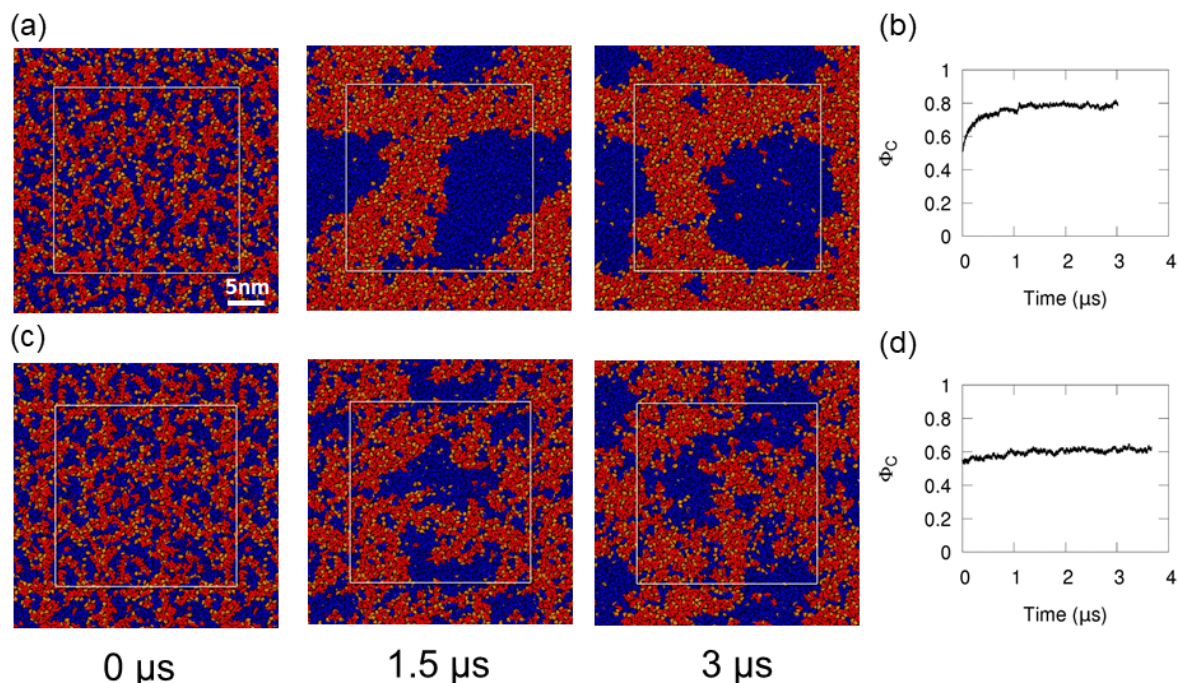


Figure 7. Phase separation simulation of SSM/DOPC/CHOL (a and b) and SSM/POPC/CHOL (c and d) mixtures. White boxes represent periodically replicated simulation boxes. (a) Snapshots of the SSM/DOPC/CHOL membrane at 0 μs , 1.5 μs , and 3 μs . Color code is as follows: red, blue, and orange represent SSM, DOPC, and CHOL, respectively. (c) Snapshots of the SSM/POPC/CHOL membrane at 0 μs , 1.5 μs , and 3 μs . Color code is as follows: red, blue, and orange represent SSM, POPC, and CHOL, respectively. (b and d) Calculated fraction of contacts between SSM and CHOL.

We also investigated ternary bilayers containing SM. It is experimentally known that this unsaturated lipid affects the domain sizes. For example, macroscopic phase separation in PSM/DOPC/CHOL was observed using fluorescence microscopy, whereas domains in a SM/POPC/CHOL mixture, which is similar in composition to the plasma membrane, could not be detected by optical microscopy⁷³⁻⁷⁵. In the present CG-MD results (Fig. 7), both mixtures showed domain formation. As Fig. 7(a) depicts, the mixture of SSM/DOPC/CHOL is clearly separated into Lo and Ld phases by creating a circular Ld domain. The fraction of contacts rapidly increased and converged at ~ 0.8 . On the other hand, SSM/POPC/CHOL

shows smaller clustering with ambiguous domain boundaries. This different phase separation behavior can be confirmed in the contact fraction plot. The fraction of contacts increases slowly, and the saturated value is much smaller than in the SSM/DOPC/CHOL case. This indicates that the phases are not clearly separated, but rather partially mixed. This result is consistent with the experimental one as nanodomains, instead of macroscopic phase separation, were only observed in the SM/POPC/CHOL mixture^{74, 76}.

To further investigate the energetics of phase separation, we calculated the free energy to transfer CHOL from water to the lipid membrane. We estimated the corresponding free energy profile along the bilayer normal using the adaptive biasing force method⁷⁷⁻⁷⁸. For the sake of faster convergence, we fixed the tilting and rotating motion of CHOL during the simulations.

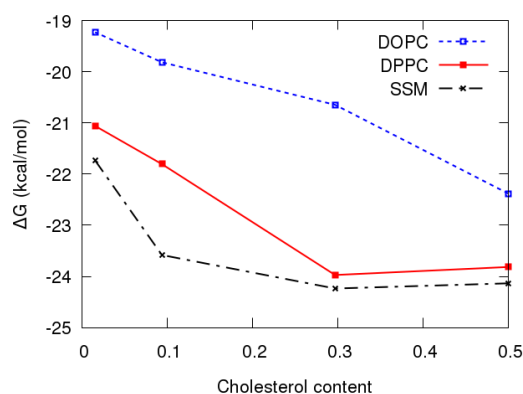


Figure 8: Calculated free energy to transfer a CHOL molecule from the aqueous solution to its equilibrium position within the lipid membrane.

Figure 8 shows the free energy required to transfer a single CHOL molecule from the aqueous solution to its equilibrium position within the lipid membrane (TFE) as a function of the CHOL concentration in the bilayer. A negative TFE indicates that CHOL prefers the lipid membrane to water. The preferred interaction between CHOL and SM can be identified from the lowest TFE values at all CHOL concentrations. With increasing the CHOL content, TFE decreases regardless of the lipid type. This indicates that CHOL prefers to reside in membranes with high CHOL content. Moreover, the TFE of CHOL in the membranes composed by saturated lipids is 2-4 kcal/mol lower than that in the DOPC membrane. This

free energy difference must be the major driving force behind the CHOL-induced phase separation into Lo and Ld domains.

CONCLUSION

In this study, we developed a novel CG lipid force field, named SPICA, for phase separation simulations. The SPICA force field has been developed using the same philosophy of a previous CG model, sometimes called SDK^{29-30, 33-36}, which satisfactorily reproduces surface/interfacial properties of lipid membranes and estimates their structural and elastic properties with a reasonable accuracy. As CHOL partitioning plays an important role in domain formation, in this new force field, we have optimized the CHOL parameters mainly focusing on improving structural properties without losing the quality of the previous model³¹ concerning thermodynamic properties. Moreover, we have developed a CG model for SM and polyunsaturated lipids. The CG parameters were adjusted to satisfy membrane properties estimated using AA-MD simulations. Especially, the 2D RDFs of the lipids within the membranes were carefully considered in the optimization to obtain a reasonable distribution of CHOLs in the membrane. Membrane properties at different CHOL concentrations showed an overall good agreement with those obtained from atomistic simulations. To further assess the SPICA force field, we simulated various ternary systems: DPPC/DOPC/CHOL, DPPC/DLiPC/CHOL, SSM/DOPC/CHOL, and SSM/POPC/CHOL bilayers. Domain separation into Lo and Ld phases was found in all systems, though the domain size and lipid distribution were fairly different depending on the lipid components. Unlike the DPPC/DOPC/CHOL bilayer, the DPPC/DLiPC/CHOL bilayer showed antiregistered domain formation, probably because of the difference in the hydrophobic thickness of the Lo and Ld lipid leaflets. The SSM/POPC/CHOL bilayer showed a smaller domain formation with more dynamic domain boundaries than the SSM/DOPC/CHOL bilayer. This is consistent with experimental observations as macroscopic phase separation was observed in a SM/DOPC/CHOL bilayer, whereas nanodomains formation was detected in a SM/POPC/CHOL bilayer. The simulation results for ternary bilayers indicate that the present CG force field can well capture the subtle differences among different ternary bilayers. We expect that the SPICA force field presented in this work will be useful in solving fundamental questions related to phase separation in lipid membranes.

Further information of the SPICA force field including tutorials and parameter files are provided at <http://www.spica-ff.org>.

Acknowledgements

We thank Profs. M. Murata, G. Fiorin, and M. L. Klein for helpful discussions. This research was supported by JSPS KAKENHI Grant Number 16H06315 and also by MEXT as "Priority Issue on Post-K computer" (Building Innovative Drug Discovery Infrastructure Through Functional Control of Biomolecular Systems). Calculations were performed on the facilities of the Research Center for Computational Science, Okazaki, the Institute for Solid State Physics, the University of Tokyo, and in part on the K-computer hosted at the RIKEN Advanced Institute for Computational Science (Proposal Nos. hp170255 and hp180191).

Supporting Information

Distributions of bond stretching and angle bending, CG order parameters, electron density profile, configuration of crystal structure of CHOL, membrane area fluctuation, 2D RDFs, and summary of the bilayer simulations.

REFERENCES

- [1] Simons, K.; Ikonen, E., Functional rafts in cell membranes. *Nature*, **1997**, *387*, 569-572.
- [2] Sezgin, E.; Levental, I.; Mayor, S.; Eggeling, C., The mystery of membrane organization: composition, regulation and roles of lipid rafts. *Nat. Rev. Mol. Cell Biol.*, **2017**, *18*, 361-374.
- [3] Engberg, O.; Hautala, V.; Yasuda, T.; Dehio, H.; Murata, M.; Slotte, J. P.; Nyholm, T. K. M., The Affinity of Cholesterol for Different Phospholipids Affects Lateral Segregation in Bilayers. *Biophys. J.*, **2016**, *111*, 546-556.
- [4] Xu, X.; London, E., The Effect of Sterol Structure on Membrane Lipid Domains Reveals How Cholesterol Can Induce Lipid Domain Formation†. *Biochemistry*, **2000**, *39*, 843-849.
- [5] Brown, D. A.; London, E., Functions of Lipid Rafts in Biological Membranes. *Annu. Rev. Cell. Dev. Biol.*, **1998**, *14*, 111-136.
- [6] Varma, R.; Mayor, S., GPI-anchored proteins are organized in submicron domains at the cell surface. *Nature*, **1998**, *394*, 798-801.

- [7] Simons, K.; Toomre, D., Lipid rafts and signal transduction. *Nat. Rev. Mol. Cell Biol.*, **2000**, *1*, 31-39.
- [8] Yang, S.-T.; Kiessling, V.; Simmons, J. A.; White, J. M.; Tamm, L. K., HIV gp41-mediated membrane fusion occurs at edges of cholesterol-rich lipid domains. *Nat. Chem. Biol.*, **2015**, *11*, 424-431.
- [9] Veatch, S. L.; Keller, S. L., Separation of Liquid Phases in Giant Vesicles of Ternary Mixtures of Phospholipids and Cholesterol. *Biophys. J.*, **2003**, *85*, 3074-3083.
- [10] Baumgart, T.; Hess, S. T.; Webb, W. W., Imaging coexisting fluid domains in biomembrane models coupling curvature and line tension. *Nature*, **2003**, *425*, 821-824.
- [11] Yuan, C.; Furlong, J.; Burgos, P.; Johnston, L. J., The Size of Lipid Rafts: An Atomic Force Microscopy Study of Ganglioside GM1 Domains in Sphingomyelin/DOPC/Cholesterol Membranes. *Biophys. J.*, **2002**, *82*, 2526-2535.
- [12] Veatch, S. L.; Polozov, I. V.; Gawrisch, K.; Keller, S. L., Liquid Domains in Vesicles Investigated by NMR and Fluorescence Microscopy. *Biophys. J.*, **2004**, *86*, 2910-2922.
- [13] Feigenson, G. W., Phase diagrams and lipid domains in multicomponent lipid bilayer mixtures. *Biochim. Biophys. Acta*, **2009**, *1788*, 47-52.
- [14] Heberle, F. A.; Wu, J.; Goh, S. L.; Petruziolo, R. S.; Feigenson, G. W., Comparison of Three Ternary Lipid Bilayer Mixtures: FRET and ESR Reveal Nanodomains. *Biophys. J.*, **2010**, *99*, 3309-3318.
- [15] Brown, D. A.; London, E., Structure and Function of Sphingolipid- and Cholesterol-rich Membrane Rafts. *J. Biol. Chem.*, **2000**, *275*, 17221-17224.
- [16] Levental, I.; Veatch, S. L., The Continuing Mystery of Lipid Rafts. *J. Mol. Biol.*, **2016**, *428*, 4749-4764.
- [17] Pike, L. J., Rafts defined: a report on the Keystone symposium on lipid rafts and cell function. *J. Lipid Res.*, **2006**, *47*, 1597-1598.
- [18] Venable, Richard M.; Sodt, Alexander J.; Rogaski, B.; Rui, H.; Hatcher, E.; MacKerell, Alexander D.; Pastor, Richard W.; Klauda, Jeffery B., CHARMM All-Atom Additive Force Field for Sphingomyelin: Elucidation of Hydrogen Bonding and of Positive Curvature. *Biophys. J.*, **2014**, *107*, 134-145.
- [19] Bera, I.; Klauda, J. B., Molecular Simulations of Mixed Lipid Bilayers with Sphingomyelin, Glycerophospholipids, and Cholesterol. *J. Phys. Chem. B*, **2017**, *121*, 5197-5208.
- [20] Jämbeck, J. P. M.; Lyubartsev, A. P., Another Piece of the Membrane Puzzle: Extending

- Slipids Further. *J. Chem. Theory Comput.*, **2012**, *9*, 774-784.
- [21] Niemelä, P. S.; Ollila, S.; Hyvönen, M. T.; Karttunen, M.; Vattulainen, I., Assessing the Nature of Lipid Raft Membranes. *PLoS Comp. Biol.*, **2007**, *3*, e34.
- [22] Sodt, Alexander J.; Pastor, Richard W.; Lyman, E., Hexagonal Substructure and Hydrogen Bonding in Liquid-Ordered Phases Containing Palmitoyl Sphingomyelin. *Biophys. J.*, **2015**, *109*, 948-955.
- [23] Marrink, S. J.; Risselada, H. J.; Yefimov, S.; Tieleman, D. P.; de Vries, A. H., The MARTINI Force Field: Coarse Grained Model for Biomolecular Simulations. *J. Phys. Chem. B*, **2007**, *111*, 7812-7824.
- [24] Melo, M. N.; Ingólfsson, H. I.; Marrink, S. J., Parameters for Martini sterols and hopanoids based on a virtual-site description. *J. Chem. Phys.*, **2015**, *143*, 243152.
- [25] Risselada, H. J.; Marrink, S. J., The molecular face of lipid rafts in model membranes. *Proc. Natl. Acad. Sci.*, **2008**, *105*, 17367-17372.
- [26] Schäfer, L. V.; Marrink, S. J., Partitioning of Lipids at Domain Boundaries in Model Membranes. *Biophys. J.*, **2010**, *99*, L91-L93.
- [27] Perlmutter, J. D.; Sachs, J. N., Interleaflet Interaction and Asymmetry in Phase Separated Lipid Bilayers: Molecular Dynamics Simulations. *J. Am. Chem. Soc.*, **2011**, *133*, 6563-6577.
- [28] Lin, X.; Lorent, J. H.; Skinkle, A. D.; Levental, K. R.; Waxham, M. N.; Gorfe, A. A.; Levental, I., Domain Stability in Biomimetic Membranes Driven by Lipid Polyunsaturation. *J. Phys. Chem. B*, **2016**, *120*, 11930-11941.
- [29] Shinoda, W.; DeVane, R.; Klein, M. L., Multi-property fitting and parameterization of a coarse grained model for aqueous surfactants. *Mol. Simulat.*, **2007**, *33*, 27-36.
- [30] Shinoda, W.; DeVane, R.; Klein, M. L., Zwitterionic Lipid Assemblies: Molecular Dynamics Studies of Monolayers, Bilayers, and Vesicles Using a New Coarse Grain Force Field. *J. Phys. Chem. B*, **2010**, *114*, 6836-6849.
- [31] MacDermaid, C. M.; Kashyap, H. K.; DeVane, R. H.; Shinoda, W.; Klauda, J. B.; Klein, M. L.; Fiorin, G., Molecular dynamics simulations of cholesterol-rich membranes using a coarse-grained force field for cyclic alkanes. *J. Chem. Phys.*, **2015**, *143*, 243144.
- [32] Davis, R. S.; Sunil Kumar, P. B.; Sperotto, M. M.; Laradji, M., Predictions of Phase Separation in Three-Component Lipid Membranes by the MARTINI Force Field. *J. Phys. Chem. B*, **2013**, *117*, 4072-4080.
- [33] Klein, M. L.; Shinoda, W., Large-Scale Molecular Dynamics Simulations of Self-

- Assembling Systems. *Science*, **2008**, *321*, 798-800.
- [34] Shinoda, W.; DeVane, R.; Klein, M. L., Coarse-grained molecular modeling of non-ionic surfactant self-assembly. *Soft Matter*, **2008**, *4*, 2454-2462.
- [35] DeVane, R.; Shinoda, W.; Moore, P. B.; Klein, M. L., Transferable Coarse Grain Nonbonded Interaction Model for Amino Acids. *J. Chem. Theory Comput.*, **2009**, *5*, 2115-2124.
- [36] Shinoda, W.; DeVane, R.; Klein, M. L., Computer simulation studies of self-assembling macromolecules. *Curr. Opin. Struct. Biol.*, **2012**, *22*, 175-186.
- [37] Phillips, J. C.; Braun, R.; Wang, W.; Gumbart, J.; Tajkhorshid, E.; Villa, E.; Chipot, C.; Skeel, R. D.; Kalé, L.; Schulten, K., Scalable molecular dynamics with NAMD. *J. Comput. Chem.*, **2005**, *26*, 1781-1802.
- [38] Klauda, J. B.; Venable, R. M.; Freites, J. A.; O'Connor, J. W.; Tobias, D. J.; Mondragon-Ramirez, C.; Vorobyov, I.; MacKerell, A. D.; Pastor, R. W., Update of the CHARMM All-Atom Additive Force Field for Lipids: Validation on Six Lipid Types. *J. Phys. Chem. B*, **2010**, *114*, 7830-7843.
- [39] Lim, J. B.; Rogaski, B.; Klauda, J. B., Update of the Cholesterol Force Field Parameters in CHARMM. *J. Phys. Chem. B*, **2011**, *116*, 203-210.
- [40] Huang, J.; MacKerell, A. D., CHARMM36 all-atom additive protein force field: Validation based on comparison to NMR data. *J. Comput. Chem.*, **2013**, *34*, 2135-2145.
- [41] Feller, S. E.; Zhang, Y.; Pastor, R. W.; Brooks, B. R., Constant pressure molecular dynamics simulation: The Langevin piston method. *J. Chem. Phys.*, **1995**, *103*, 4613-4621.
- [42] Darden, T.; York, D.; Pedersen, L., Particle mesh Ewald: An $N \cdot \log(N)$ method for Ewald sums in large systems. *J. Chem. Phys.*, **1993**, *98*, 10089-10092.
- [43] Essmann, U.; Perera, L.; Berkowitz, M. L.; Darden, T.; Lee, H.; Pedersen, L. G., A smooth particle mesh Ewald method. *J. Chem. Phys.*, **1995**, *103*, 8577-8593.
- [44] Lee, J.; Cheng, X.; Swails, J. M.; Yeom, M. S.; Eastman, P. K.; Lemkul, J. A.; Wei, S.; Buckner, J.; Jeong, J. C.; Qi, Y.; Jo, S.; Pande, V. S.; Case, D. A.; Brooks, C. L.; MacKerell, A. D.; Klauda, J. B.; Im, W., CHARMM-GUI Input Generator for NAMD, GROMACS, AMBER, OpenMM, and CHARMM/OpenMM Simulations Using the CHARMM36 Additive Force Field. *J. Chem. Theory Comput.*, **2015**, *12*, 405-413.
- [45] Plimpton, S., Fast Parallel Algorithms for Short-Range Molecular Dynamics. *J. Comput. Phys.*, **1995**, *117*, 1-19.

- [46] Nosé, S., A unified formulation of the constant temperature molecular dynamics methods. *J. Chem. Phys.*, **1984**, *81*, 511-519.
- [47] Hoover, W. G., Canonical dynamics: Equilibrium phase-space distributions. *Phys. Rev. A*, **1985**, *31*, 1695-1697.
- [48] Parrinello, M.; Rahman, A., Crystal Structure and Pair Potentials: A Molecular-Dynamics Study. *Phys. Rev. Lett.*, **1980**, *45*, 1196-1199.
- [49] Parrinello, M.; Rahman, A., Polymorphic transitions in single crystals: A new molecular dynamics method. *J. Appl. Phys.*, **1981**, *52*, 7182-7190.
- [50] Hockney, R. W.; Eastwood, J. W., *Computer simulation using particles*. Special student ed.; A. Hilger: Bristol England ; Philadelphia, 1988.
- [51] Humphrey, W.; Dalke, A.; Schulten, K., VMD: Visual molecular dynamics. *J. Mol. Graphics*, **1996**, *14*, 33-38.
- [52] Oliphant, T. E., Python for Scientific Computing. *Comput. Sci. Eng.*, **2007**, *9*, 10-20.
- [53] Michaud-Agrawal, N.; Denning, E. J.; Woolf, T. B.; Beckstein, O., MDAAnalysis: A toolkit for the analysis of molecular dynamics simulations. *J. Comput. Chem.*, **2011**, *32*, 2319-2327.
- [54] Bennett, W. F. D.; MacCallum, J. L.; Hinner, M. J.; Marrink, S. J.; Tieleman, D. P., Molecular View of Cholesterol Flip-Flop and Chemical Potential in Different Membrane Environments. *J. Am. Chem. Soc.*, **2009**, *131*, 12714-12720.
- [55] Shinoda, W.; Okazaki, S., A Voronoi analysis of lipid area fluctuation in a bilayer. *J. Chem. Phys.*, **1998**, *109*, 1517-1521.
- [56] Hsu, L.-Y.; Kampf, J. W.; Nordman, C. E., Structure and pseudosymmetry of cholesterol at 310 K. *Acta Crystallogr. Sect. B: Struct. Sci.*, **2002**, *58*, 260-264.
- [57] Hung, W.-C.; Lee, M.-T.; Chen, F.-Y.; Huang, H. W., The Condensing Effect of Cholesterol in Lipid Bilayers. *Biophys. J.*, **2007**, *92*, 3960-3967.
- [58] Ipsen, J. H.; Mouritsen, O. G.; Bloom, M., Relationships between lipid membrane area, hydrophobic thickness, and acyl-chain orientational order. The effects of cholesterol. *Biophys. J.*, **1990**, *57*, 405-412.
- [59] Drolle, E.; Kučerka, N.; Hoopes, M. I.; Choi, Y.; Katsaras, J.; Karttunen, M.; Leonenko, Z., Effect of melatonin and cholesterol on the structure of DOPC and DPPC membranes. *Biochim. Biophys. Acta*, **2013**, *1828*, 2247-2254.
- [60] Rawicz, W.; Smith, B. A.; McIntosh, T. J.; Simon, S. A.; Evans, E., Elasticity, Strength, and Water Permeability of Bilayers that Contain Raft Microdomain-Forming Lipids.

Biophys. J., **2008**, *94*, 4725-4736.

- [61] Tierney, K. J.; Block, D. E.; Longo, M. L., Elasticity and Phase Behavior of DPPC Membrane Modulated by Cholesterol, Ergosterol, and Ethanol. *Biophys. J.*, **2005**, *89*, 2481-2493.
- [62] Martinez-Seara, H.; Róg, T.; Karttunen, M.; Vattulainen, I.; Reigada, R., Cholesterol Induces Specific Spatial and Orientational Order in Cholesterol/Phospholipid Membranes. *PLoS ONE*, **2010**, *5*, e11162.
- [63] Wang, E.; Klauda, J. B., Examination of Mixtures Containing Sphingomyelin and Cholesterol by Molecular Dynamics Simulations. *J. Phys. Chem. B*, **2017**, *121*, 4833-4844.
- [64] Leventis, R.; Silvius, J. R., Use of Cyclodextrins to Monitor Transbilayer Movement and Differential Lipid Affinities of Cholesterol. *Biophys. J.*, **2001**, *81*, 2257-2267.
- [65] Backer, J. M.; Dawidowicz, E. A., Transmembrane movement of cholesterol in small unilamellar vesicles detected by cholesterol oxidase. *J. Biol. Chem.*, **1981**, *256*, 586-8.
- [66] Garg, S.; Porcar, L.; Woodka, A. C.; Butler, P. D.; Perez-Salas, U., Noninvasive Neutron Scattering Measurements Reveal Slower Cholesterol Transport in Model Lipid Membranes. *Biophys. J.*, **2011**, *101*, 370-377.
- [67] Brasaemle, D. L.; Robertson, A. D.; Attie, A. D., Transbilayer movement of cholesterol in the human erythrocyte membrane. *J. Lipid Res.*, **1988**, *29*, 481-9.
- [68] Jo, S.; Rui, H.; Lim, J. B.; Klauda, J. B.; Im, W., Cholesterol Flip-Flop: Insights from Free Energy Simulation Studies. *J. Phys. Chem. B*, **2010**, *114*, 13342-13348.
- [69] Parisio, G.; Sperotto, M. M.; Ferrarini, A., Flip-Flop of Steroids in Phospholipid Bilayers: Effects of the Chemical Structure on Transbilayer Diffusion. *J. Am. Chem. Soc.*, **2012**, *134*, 12198-12208.
- [70] Marrink, S. J.; de Vries, A. H.; Harroun, T. A.; Katsaras, J.; Wassall, S. R., Cholesterol Shows Preference for the Interior of Polyunsaturated Lipid Membranes. *J. Am. Chem. Soc.*, **2008**, *130*, 10-11.
- [71] Sapay, N.; Bennett, W. F. D.; Tieleman, D. P., Thermodynamics of flip-flop and desorption for a systematic series of phosphatidylcholine lipids. *Soft Matter*, **2009**, *5*, 3295-3302.
- [72] Levental, Kandice R.; Lorent, Joseph H.; Lin, X.; Skinkle, Allison D.; Surma, Michal A.; Stockenbojer, Emily A.; Gorfe, Alemayehu A.; Levental, I., Polyunsaturated Lipids Regulate Membrane Domain Stability by Tuning Membrane Order. *Biophys. J.*, **2016**,

110, 1800-1810.

- [73] Feigenson, G. W., Phase Boundaries and Biological Membranes. *Annu. Rev. Biophys. Biomol. Struct.*, **2007**, *36*, 63-77.
- [74] Petruzielo, R. S.; Heberle, F. A.; Drazba, P.; Katsaras, J.; Feigenson, G. W., Phase behavior and domain size in sphingomyelin-containing lipid bilayers. *Biochim. Biophys. Acta*, **2013**, *1828*, 1302-1313.
- [75] Zhao, J.; Wu, J.; Shao, H.; Kong, F.; Jain, N.; Hunt, G.; Feigenson, G., Phase studies of model biomembranes: Macroscopic coexistence of $L\alpha+L\beta$, with light-induced coexistence of $L\alpha+L\alpha$ Phases. *Biochim. Biophys. Acta*, **2007**, *1768*, 2777-2786.
- [76] Pathak, P.; London, E., Measurement of Lipid Nanodomain (Raft) Formation and Size in Sphingomyelin/POPC/Cholesterol Vesicles Shows TX-100 and Transmembrane Helices Increase Domain Size by Coalescing Preexisting Nanodomains But Do Not Induce Domain Formation. *Biophys. J.*, **2011**, *101*, 2417-2425.
- [77] Darve, E.; Rodríguez-Gómez, D.; Pohorille, A., Adaptive biasing force method for scalar and vector free energy calculations. *J. Chem. Phys.*, **2008**, *128*, 144120.
- [78] Hénin, J. r.; Fiorin, G.; Chipot, C.; Klein, M. L., Exploring Multidimensional Free Energy Landscapes Using Time-Dependent Biases on Collective Variables. *J. Chem. Theory Comput.*, **2010**, *6*, 35-47.

for Table of Contents use only

SPICA Force Field for Lipid Membranes: Domain Formation Induced by Cholesterol

Sangjae Seo and Wataru Shinoda

